GMR
The Original

FABRICATION OF POLYMERIC (STARCH/PVA) ELECTROSPUN NANOSCAFFOLDS INCORPORATED WITH ULTRASONIC-ASSISTED BIOGENIC SYNTHESIS OF CUO NANOPARTICLES FROM BROWN MARINE MACROALGAE (DICTYOTA SP.) EXTRACT

Elsa Sharon Emarald Ruban[1], Harish Manoharan[2], Nishandhini Marimuthu[3], Anguchamy Veeruraj[4], Kaliyamoorthy Dass[5*]

[1]Saveetha Medical College & Hospital (SMCH), Saveetha Institute of Medical and Technical Sciences (SIMATS), Thandalam, Chennai, Tamil Nadu 602105, India. elsasharon2004@gmail.com
[2]Department of Microbiology, Saveetha Medical College and Hospital, Saveetha Institute of Medical And Technical Sciences (SIMATS), Thandalam, Chennai-602105, Tamil Nadu, India. manoharan.harish@gmail.com, https://orcid.org/0000-0002-8613-7440
[3]Department of Bioinformatics, School of Life Sciences, Vels Institute of Science Technology and Advanced Studies, Pallavaram, Chennai-600117, Tamil Nadu, India. Email: enishay30@gmail.com; ORCID: https://orcid.org/0000-0002-8536-4473
[4]Saveetha Institute of Basic Medical Sciences (SIBMS), Saveetha Medical College and Hospital, Saveetha Institute of Medical and Technical Sciences (SIMATS), Saveetha University, Chennai, 602 105, Tamil Nadu, India. anguveeruraj@gmail.com, https://orcid.org/0000-0001-7456-6507
[5*]Natural Product and Vector Control Research Lab, Department of Pharmacology, Saveetha Medical College and Hospital, Saveetha Institute of Medical And Technical Sciences (SIMATS), Thandalam, Chennai-602105, Tamil Nadu, India. dass.smc@saveetha.com; kdassrsgc1987@gmail.com, https://orcid.org/0000-0002-4564-3275

ABSTRACT

This study presents an eco-friendly strategy for synthesizing copper oxide nanoparticles (CuO NPs) using the brown marine algae Dictyota as a biogenic source. The ultrasonic-assisted extraction of algal bioactives facilitated efficient nanoparticle formation, which was confirmed by UV–Vis, Fourier-transform infrared spectroscopy (FTIR), X-ray diffraction (XRD), Scanning electron microscopy (SEM), Dynamic light scattering (DLS), and zeta potential analyses. The synthesized CuO NPs were incorporated into a starch/polyvinyl alcohol (PVA) matrix to fabricate electrospun nanofibrous scaffolds with enhanced structural integrity and biological functionality. Physicochemical characterization revealed uniform fiber morphology, strong thermal stability, and successful nanoparticle integration. The antimicrobial potential of the scaffolds was evaluated against pathogenic bacterial and fungal strains, demonstrating significant inhibitory effects. This work highlights the synergistic benefits of green synthesis and polymeric nanofiber technology, proposing a sustainable and biocompatible platform for antimicrobial applications. Overall, the study contributes to the advancement of marine-derived nanomaterials and their potential in biomedical and environmental fields.

KEYWORDS: Dictyota sp., Green synthesis, CuO nanoparticles, Starch/PVA nanoscaffolds, Antimicrobial activity.

1. INTRODUCTION

Marine ecosystems are a rich reservoir of biologically active compounds, offering unique opportunities for the development of novel materials with therapeutic, environmental, and industrial applications [1]. Among marine flora, brown algae (Phaeophyceae) have received increasing attention due to their diverse phytochemical constituents, including terpenoids, polyphenols, sulfated polysaccharides, and proteins [2]. These compounds have been reported to exhibit antioxidant, antimicrobial, anti-inflammatory, and anticancer activities, making marine algae an attractive source for green synthesis of nanomaterials [3]. In this context, Dictyota, a genus of brown macroalgae commonly found along tropical and subtropical coastlines, has emerged as a promising candidate for eco-friendly nanomaterial fabrication due to its rich content of secondary metabolites and easy accessibility [4].

The growing demand for sustainable and biocompatible materials has driven the advancement of green nanotechnology [5]. This discipline focuses on the biosynthesis of nanoparticles using biological sources, thus avoiding the use of toxic reducing agents and stabilizers typically associated with chemical synthesis [6]. Among various nanomaterials, copper oxide nanoparticles (CuO NPs) have attracted considerable interest due to their distinctive physicochemical and biological properties, such as high thermal stability, catalytic efficiency, and potent antimicrobial activity [7]. CuO NPs have been employed in several biomedical and environmental applications, including drug delivery, biosensing, wound healing, and wastewater treatment [8]. However, to enhance their practical application, especially in biomedical fields, it is essential to incorporate these nanoparticles into biocompatible and biodegradable matrices that can support their stability and targeted delivery [9].

Electrospinning is a versatile and cost-effective technique for fabricating nanofibrous scaffolds that closely mimic the natural extracellular matrix (ECM) of biological tissues [10]. These nanofibers provide a high surface-to-

volume ratio, porous structure, and tunable mechanical properties, making them ideal for applications such as tissue engineering, wound dressing, and controlled drug release [11]. Biopolymers like starch and polyvinyl alcohol (PVA) have been widely explored for scaffold development due to their biodegradability, biocompatibility, and excellent film-forming properties [12]. Starch, a natural polysaccharide, offers favorable biological interactions, while PVA provides mechanical strength and thermal stability [13]. Blending starch with PVA and reinforcing it with functional nanoparticles like CuO creates multifunctional scaffolds with improved structural and biological performance [14].

This study integrates the potential of marine algae-mediated green synthesis with the fabrication of polymeric electrospun nanofibers for developing a novel antimicrobial platform [15]. The brown seaweed Dictyota collected from the coastal region of Rameswaram, Tamil Nadu, India, was employed as a biogenic source for the synthesis of CuO NPs via an ultrasonic-assisted extraction method [16]. Ultrasonication was chosen to enhance the yield and quality of bioactive compounds through cell wall disruption and effective mass transfer [17]. The bio-reduced CuO NPs were then incorporated into a starch/PVA matrix, and electrospun to produce nanofibrous scaffolds using an optimized electrospinning setup [18]. The choice of using a green synthesis approach ensures environmental safety, while the electrospun architecture offers enhanced interaction with microbial cells, potentially improving the antimicrobial efficacy [19].

2. MATERIALS AND METHODS

2.1 Chemicals and reagents

For this study, the brown seaweed Dictyota was gathered from the shoreline of Rameswaram, Tamil Nadu, India, to support the eco-conscious production of CuO NPs. Copper (II) sulfate pentahydrate ($CuSO_4 \cdot 5H_2O$), of analytical grade, was used as the copper source. PVA (molecular weight ~115,000 g/mol) and starch were utilized to fabricate biocompatible scaffolds. Electrospinning was carried out using a HOLMARC HO-NFES-040 unit. All chemicals and solvents used, sourced from Merck and Sigma-Aldrich, were of analytical grade to ensure reliability. Characterization included UV–Vis spectroscopy, Fourier-transform infrared spectroscopy (FTIR), X-ray diffraction (XRD), Scanning electron microscopy (SEM), Dynamic light scattering (DLS), zeta potential, and Thermogravimetric analysis (TGA).

2.2 Collection and preparation of marine algae

Dictyota samples were freshly harvested from intertidal regions near Rameswaram's coast. The algae were chilled during transportation to maintain integrity. Initial cleaning involved rinsing thoroughly with tap water to eliminate sand, epiphytes, and surface debris, followed by several rinses with distilled water to clear remaining salts and impurities. A 100 g portion of the cleaned algae was cut into even fragments and air-dried under room conditions for two weeks. Once dried, the material was finely ground using a mechanical grinder and stored in sealed containers for future extraction and synthesis processes.

2.3 Extraction of bioactive components using ultrasonication

To extract bioactive phytoconstituents from Dictyota, ultrasonic-assisted extraction (UAE) was utilized. Two grams of powdered algae were mixed with 50 mL Milli-Q water in a 100 mL borosilicate container. The mixture was treated using a LABQUEST ultrasonic cleaner (Borosil; Serial No. 941032329018) at 60°C for 45 minutes to facilitate cell disruption and enhance extraction. The extract was then filtered through sterile Whatman No. 1 filter paper to eliminate particulates. The filtrate was stored in sterile conditions at 10°C. A portion was freeze-dried using a lyophilizer to obtain a powdered extract for future nanoparticle synthesis [20, 21].

2.4 Biosynthesis of CuO NPs

CuO NPs were synthesized by reacting the Dictyota extract with copper sulfate solution. A 0.1 M $CuSO_4 \cdot 5H_2O$ solution (50 mL) was prepared and combined with 10 mL of the algal extract (10 mg in 10 mL Milli-Q water), keeping a 5:1 volume ratio. The reaction mixture was stirred continuously at 650 rpm and heated at 60°C for 2 hours using a magnetic stirrer with a hot plate. A visible color transition from deep blue to bluish-green indicated CuO NP formation, driven by phytochemical reduction of Cu^{2+} ions. The particles were washed thrice with distilled water and freeze-dried for 48 hours to yield a powder for analysis and scaffold development [22].

2.5 Electrospinning of starch/PVA scaffolds loaded with CuO NPs

A 15% (w/w) PVA aqueous solution was prepared by dissolving fully hydrolyzed PVA in Milli-Q water under continuous stirring and mild heating at 50°C. After dissolution, 100 mg of starch and 100 mg of CuO NPs were added. The mixture was stirred vigorously at 50°C for 2.5 hours to ensure uniform blending. This homogeneous solution was then loaded into a syringe fitted with a stainless steel needle (internal diameter 0.84 mm). Using the HOLMARC HO-NFES-040 device, electrospinning was performed at 11.5 kV, a 12.3 cm needle-to-collector gap, and a 0.4 mL/h feed rate. The process ran for 6–8 hours at ambient temperature, producing nanofibrous mats, which were stored in desiccators for later use [23-25].

2.6 Physicochemical characterization

2.6.1 Ultraviolet–visible spectroscopy analysis

The UV–Vis spectral profiles of the algal extract, CuO NPs, and CuO-loaded scaffolds were recorded to examine optical features and validate nanoparticle synthesis. A VIS SPEC V-730 UV–Vis spectrophotometer was used to scan samples from 200–800 nm, with deionized water as a blank. Peaks in the 270–300 nm range confirmed surface plasmon resonance (SPR), characteristic of CuO NPs, and supported nanoparticle incorporation into the scaffold matrix [26].

2.6.2 FTIR spectroscopy analysis

FTIR spectroscopy identified functional groups and molecular interactions. Spectra of the Dictyota extract, CuO NPs, and CuO-loaded scaffolds were obtained using a PerkinElmer Spectrum Two spectrometer in ATR mode. Spectra were recorded from 4000 to 400 cm^{-1} at 4 cm^{-1} resolution with 64 scans per sample. Key peaks corresponding to O–H, C=O, amide groups, and metal–oxygen bonds confirmed the successful integration of biomolecules and metal oxides within the polymer [27].

2.6.3 XRD analysis

XRD was carried out using a Bruker D8 Advance instrument with CuKα radiation (λ = 1.5406 Å), operating at 40 kV and 40 mA. Samples were scanned from 5° to 90° 2θ with a step size of 0.029649°. Distinct diffraction peaks indicated monoclinic CuO crystal structure. Shifts or broadening in scaffold patterns verified nanoparticle incorporation into the matrix [28].

2.6.4 SEM analysis

The morphology of CuO NPs within the starch/PVA scaffold was visualized using a JEOL JSM-IT800 NANO SEM. Samples were coated with a gold layer to minimize charging. Images showed the fiber uniformity, texture, and nanoparticle dispersion. Electrospun fibers were continuous with well-distributed CuO particles, validating effective electrospinning and embedding [29].

2.6.5 TGA

Thermal stability was analyzed with a PerkinElmer TGA 8000. Approximately 5 mg of each sample was heated from room temperature to 550°C at 15°C/min in a nitrogen atmosphere. Thermograms revealed stages of decomposition—initial water loss, polymer degradation, and nanoparticle stabilization. CuO NPs enhanced the scaffold's thermal resistance, supporting their structural reinforcement role [30].

2.6.6 Zeta potential and particle size analysis

Colloidal stability and size of CuO NPs were assessed using a Malvern Zetasizer Ultra. DLS determined hydrodynamic particle size, while zeta potential indicated surface charge. Values exceeding ±30 mV suggested high particle stability due to repulsive electrostatic interactions. These parameters are crucial for predicting in vivo nanoparticle dispersion and performance [40].

All raw and interpreted data were deposited in the Mendeley Data repository (DOI: 10.17632/xtwhbc25hj.1) to support reproducibility and data integrity.

2.7. Evaluation of antimicrobial properties

The antimicrobial efficacy of Dictyota extract, CuO NPs, and starch/PVA electrospun nanoscaffolds (each at 50 µg/mL) was evaluated using the agar well diffusion method. The test organisms included bacterial strains (Escherichia coli, Klebsiella pneumoniae, Staphylococcus aureus, Citrobacter koseri) and fungal species (Aspergillus niger, Penicillium sp.). Bacterial suspensions were standardized to 0.5 McFarland (~1.5×10^8 CFU/mL) and inoculated onto Mueller-Hinton agar, while fungal spores were inoculated onto Sabouraud dextrose agar. Wells (6 mm) were created, and 50 µL of each sample was loaded. Ciprofloxacin and voriconazole served as positive controls for bacterial and fungal assays, respectively. Plates were pre-diffused for 30 minutes, then incubated—bacteria at 37°C for 24 hours, fungi at 28°C for 48 hours. Antimicrobial activity was assessed by measuring inhibition zone diameters in millimeters. All tests were performed in triplicate to ensure reproducibility and statistical reliability [31, 32].

2.8. Statistical processing

All statistical analyses were conducted using SPSS version 25.0 and GraphPad Prism version 9.0. Experimental results were presented as mean ± standard deviation (SD), derived from three independent replicates. One-way ANOVA was performed to identify significant differences between groups, followed by post hoc Tukey's or Dunnett's test. A p-value below 0.05 indicated statistical significance. Pearson's correlation and Shapiro-Wilk tests were used to determine associations and normality. Data not conforming to normality were log-transformed before analysis [33].

3. RESULTS

3.1. UV–visible spectroscopy

The UV–Visible absorption profiles of the aqueous Dictyota extract and the synthesized CuO NPs (Figure 1) were recorded using a JASCO V-730 spectrophotometer across 200–800 nm with 1 nm resolution. The algal extract displayed a broad absorption curve with increasing absorbance from 800 nm to 200 nm, peaking at 1.482 at 337 nm, indicating the presence of polyphenolic or flavonoid compounds contributing to nanoparticle formation and stability. Conversely, the CuO NPs exhibited a clear absorption peak around 270–300 nm, signifying the surface plasmon resonance (SPR) characteristic of CuO NPs, thereby confirming successful nanoparticle synthesis. This

absorption region is consistent with the reported optical behavior of monoclinic CuO nanoparticles, which display strong interband transitions near 270–330 nm due to $O^{2-} \rightarrow Cu^{2+}$ charge transfer. The absence of additional peaks between 450–600 nm—which are typical of Cu_2O—indicates that no mixed-phase Cu_2O/CuO formation occurred. This conclusion is further corroborated by XRD results (Section 3.3), confirming the monoclinic CuO phase (JCPDS No. 48-1548). The CuO NPs showed a markedly higher absorbance, reaching 2.369 at 800 nm, tapering toward shorter wavelengths, consistent with the known optical traits of metal oxide nanoparticles. The algal extract lacked sharp peaks, while the CuO spectrum showed a strong SPR band, indicating successful transformation through the biosynthetic process. These findings confirm that the Dictyota extract effectively mediated CuO NPs formation, supporting further exploration of their application in polymeric scaffolds.

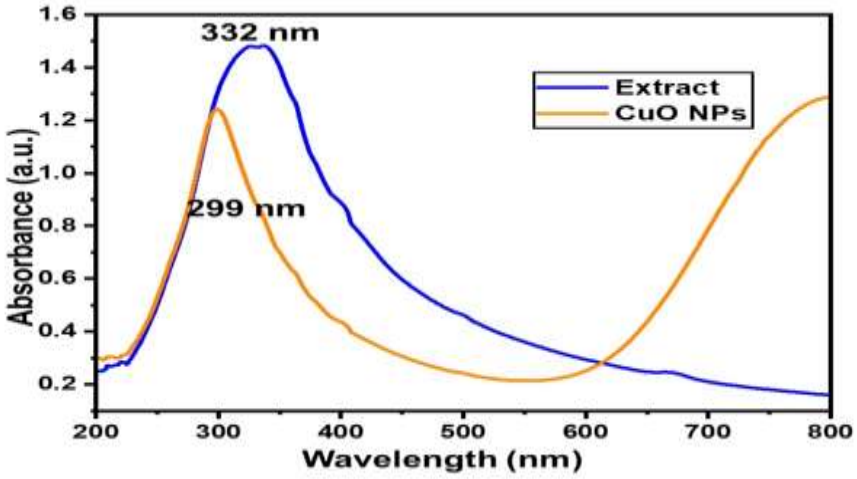

Figure 1. UV–Visible spectral profiles of algal extract and CuO NPs.

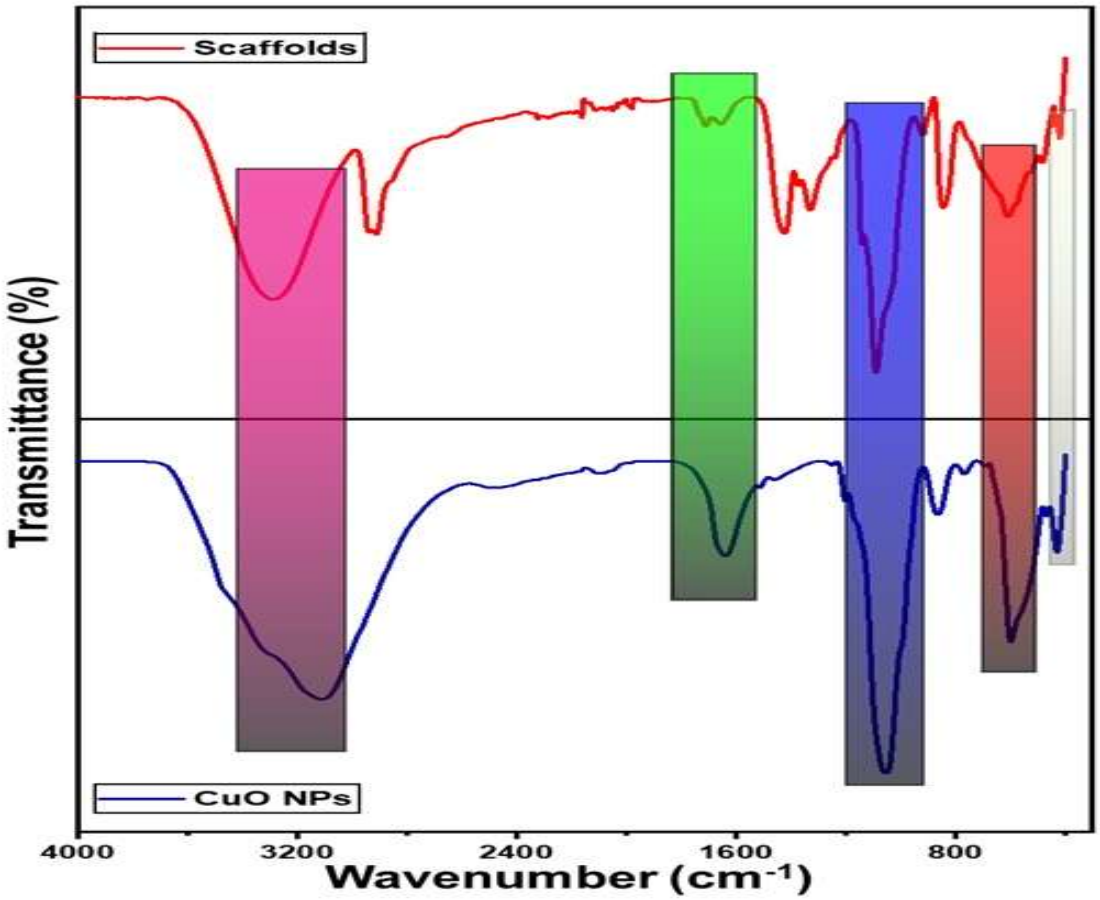

Figure 2. FTIR spectra of CuO NPs and their incorporation into nanoscaffolds.

3.2. FTIR spectroscopy analysis

FTIR analysis (Figure 2) of the synthesized CuO NPs and CuO NP-loaded starch/PVA nanoscaffolds revealed significant functional groups and chemical interactions. The CuO NPs displayed peaks at 2033.36 cm^{-1}, 1640.64 cm^{-1}, and 594.02 cm^{-1}, associated with Cu–O stretching vibrations, verifying CuO formation. Peaks at 767.66 cm^{-1} and 469.77 cm^{-1} further supported the presence of Cu–O bonds. The scaffold spectrum exhibited notable bands at 3289.72 cm^{-1} (O–H stretching of starch/PVA), 1426.07 cm^{-1} (C–H bending), and 110.59 cm^{-1} (C–O–C

linkages), indicating the structural presence of the polymer. Additional peaks between 600–400 cm^{-1} confirmed CuO NPs incorporation through interactions with hydroxyl and carbonyl moieties. These observations validate successful functional integration of CuO NPs into the polymeric matrix, while retaining critical chemical bonds essential for biomedical application viability.

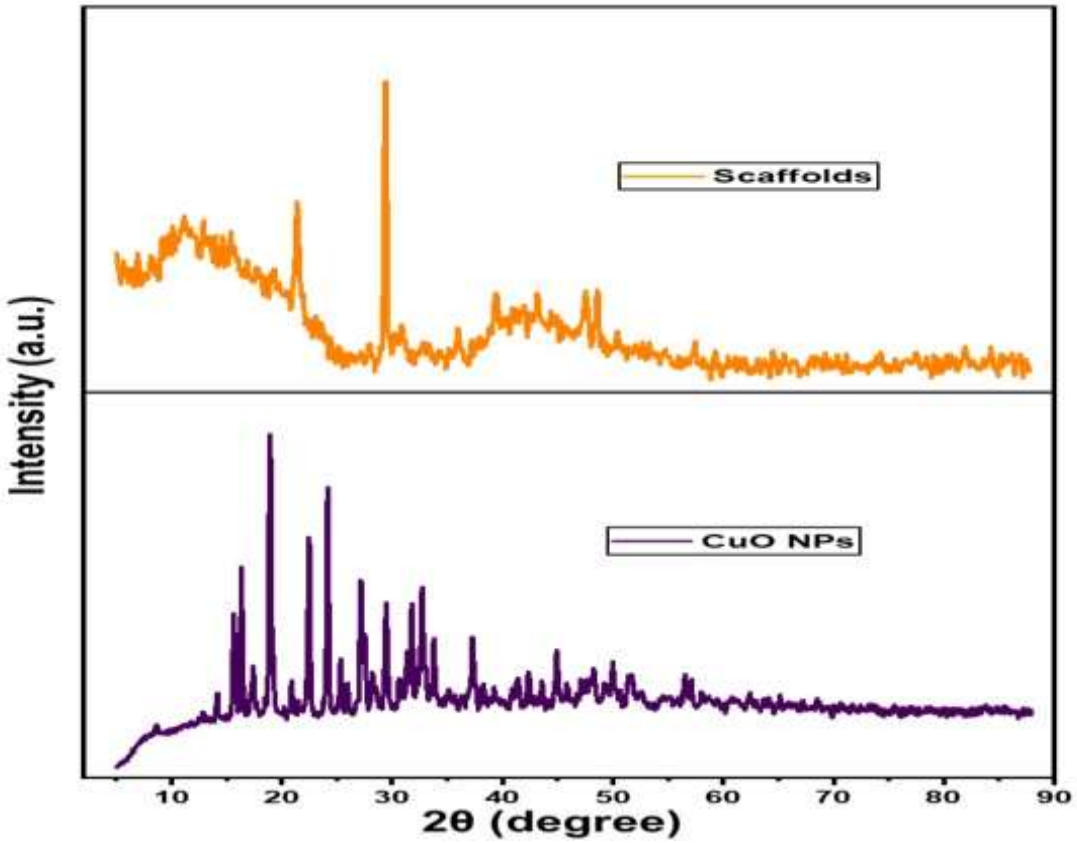

Figure 3. XRD patterns of synthesized CuO NPs and CuO-loaded scaffolds.

3.3. XRD analysis

XRD characterization of the synthesized CuO NPs and nanoscaffolds (Figure 3) highlighted distinct crystallographic signatures. The CuO NPs presented sharp peaks at 14.030°, 15.601°, 16.255°, 17.237°, 18.807°, 20.901°, 22.341°, 24.173°, 25.416°, and 32.745° (2θ), aligning with the monoclinic CuO phase (JCPDS No. 48-1548), with the dominant peak at 24.173° (d = 3.68 Å, 100% intensity). The calculated d-spacings (e.g., 6.31 Å, 5.68 Å, 4.71 Å, 2.73 Å) confirmed crystalline structure. Nanoscaffolds showed strong peaks at 21.346° (4.16 Å, 49.5%) and 29.298° (3.05 Å, 100%), corresponding to the starch/PVA matrix, with weaker reflections at 35.778° (2.51 Å) and 48.516° (1.87 Å) confirming CuO NP presence. Peak broadening (FWHM = 0.1°–0.6°) in the scaffold signified reduced crystallinity due to polymer–NP interactions. These results affirm successful synthesis of crystalline CuO NPs and their incorporation into the polymeric framework, preserving structural stability for biomedical use.

3.4. SEM analysis

SEM imaging (Figure 4) of synthesized CuO NPs and CuO-integrated starch/PVA scaffolds revealed distinguishable morphologies. The CuO NPs displayed mainly spherical to irregular shapes with visible agglomeration, likely caused by their elevated surface energy. The nanoscaffolds showed a consistent, interconnected fibrous architecture, with fiber diameters in the nanometric scale, confirming proper electrospinning. CuO NPs appeared evenly distributed across the scaffold as bright dots, validating uniform embedding without substantial clumping. The fiber surfaces were largely smooth with subtle texture, indicating compatibility between nanoparticles and the polymer blend. Low bead frequency and uniform diameter across fibers reflected optimized spinning conditions. These findings verify structural fidelity and effective dispersion of CuO NPs within the scaffold, crucial for both mechanical robustness and functional efficacy in biomedical settings.

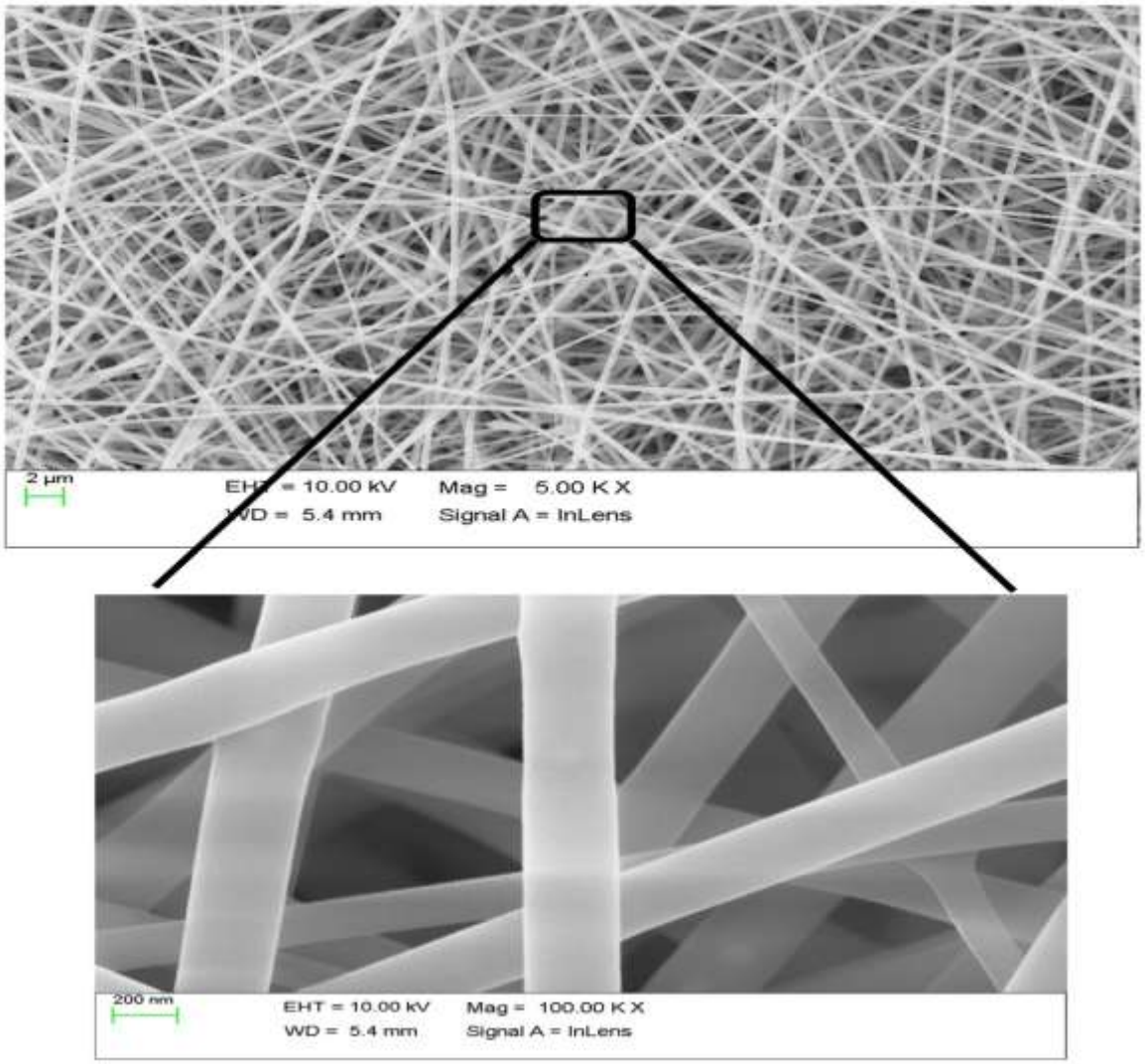

Figure 4. SEM analysis of synthesized CuO NPs and CuO-loaded scaffolds.

3.5. TGA

TGA results for CuO NP-loaded scaffolds (Figure 5) showed a distinct multi-phase thermal degradation under a nitrogen atmosphere. The 5.502 mg sample initially lost 7.301% weight below 101.7°C, attributed to moisture release. Major degradation occurred from 234.95°C to 377.09°C, peaking at 324.79°C, indicating breakdown of starch/PVA chains with a 37.368% mass loss. Further weight loss past 400°C suggested char formation and stabilization by CuO NPs, which delayed degradation and boosted thermal resistance. Residual mass retention at elevated temperatures confirmed CuO NPs' role as thermal reinforcers. Degradation completed at 548.4°C. These observations validate the role of CuO NPs in enhancing the scaffold's thermal durability, proving their suitability for applications demanding thermal stability.

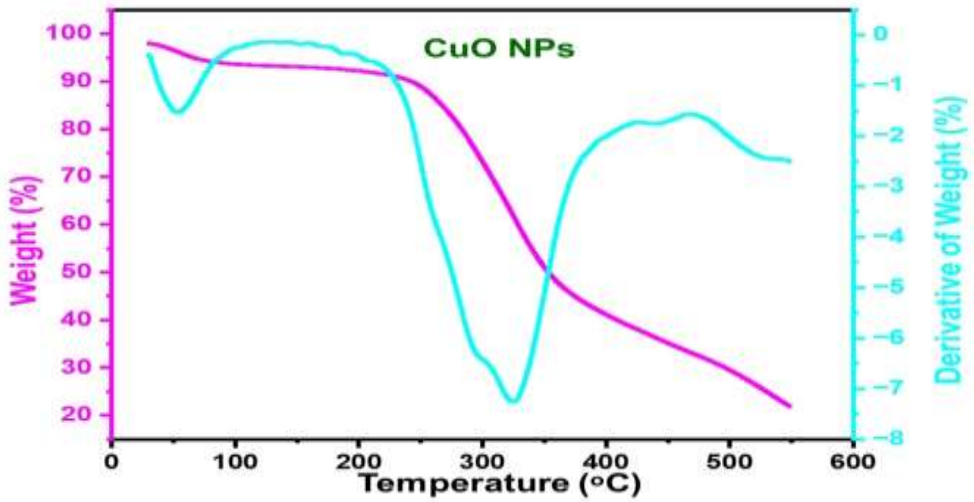

Figure 5. Thermal degradation behavior of CuO-incorporated nanoscaffolds.

3.6. Zeta potential and particle size analysis

DLS and zeta potential analysis of biosynthesized CuO NPs revealed essential colloidal characteristics. Particle size distribution (by intensity) yielded a Z-average of 92.8 nm (Figure 6) and a polydispersity index (PDI) of 0.688, reflecting moderate size dispersion. Zeta potential measurements (Figure 7) showed an average surface charge of −20.08 mV, with two peaks at −37.52 mV and −16.29 mV, indicating heterogeneous colloidal populations. The dominant −37.52 mV peak implied adequate repulsion to hinder aggregation, while the −16.29 mV signal hinted at partial instability. Conductivity (0.0343 mS/cm) and quality factor (6.538) verified measurement reliability. These findings suggest moderate nanoparticle stability in aqueous systems, with negative zeta potential supporting biocompatibility. Particle size variation may reflect a mix of aggregated and discrete NPs, emphasizing the need for further formulation refinement to ensure dispersion uniformity.

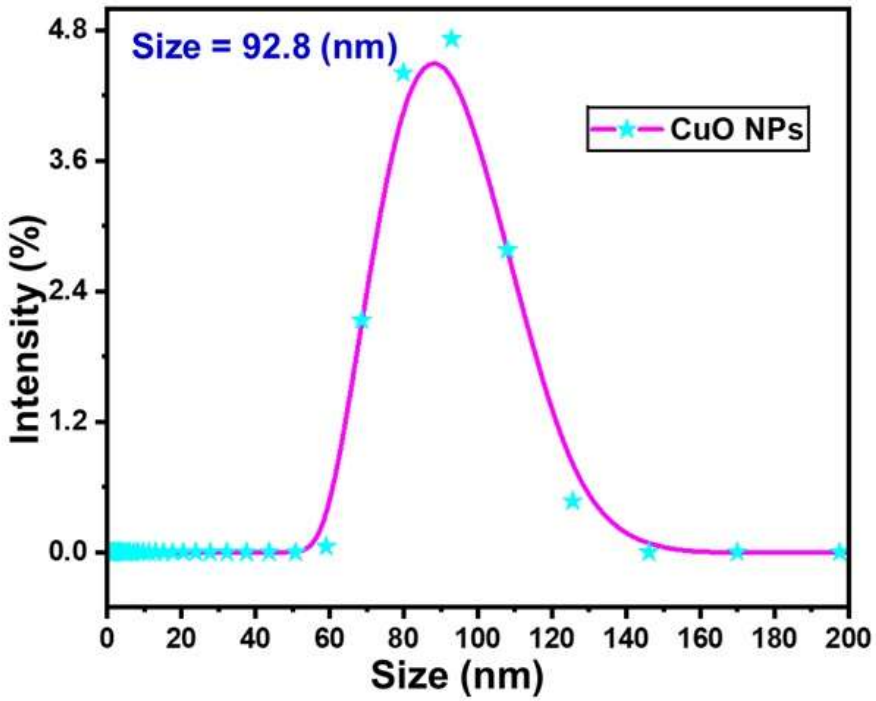

Figure6. DLS particles size analysis of CuO NPs

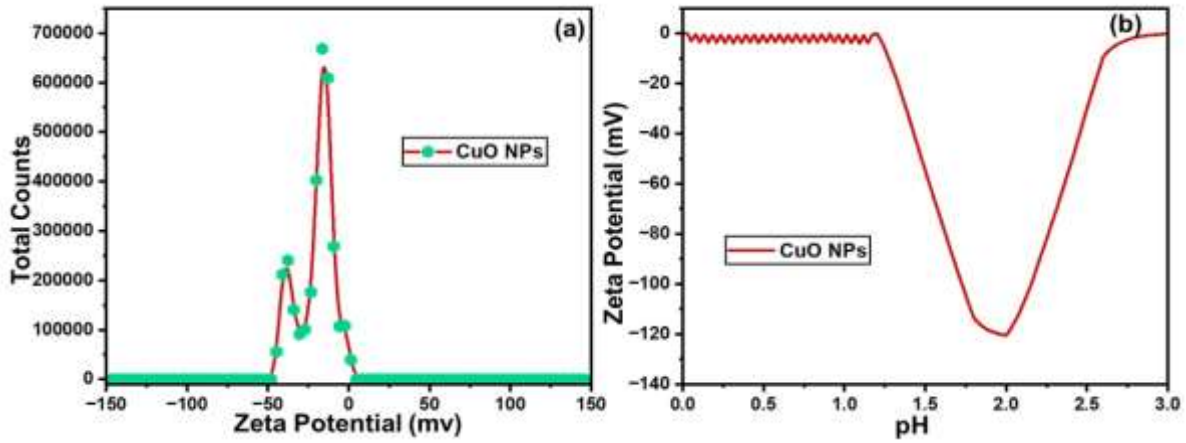

Figure7. Zeta-potential analysis of CuO NPs

3.7. Evaluation of antimicrobial activity

The antimicrobial efficacy of Dictyota extract, CuO NPs, and starch/PVA electrospun nanoscaffolds was evaluated at 50 µg/mL against a panel of pathogenic microorganisms (Table 1). The Dictyota extract demonstrated moderate activity, with inhibition zones of 18±0.18 mm for Escherichia coli, 16±0.32 mm for Klebsiella pneumoniae, 14±0.13 mm for Staphylococcus aureus, and 18±0.12 mm for Citrobacter koseri, indicating broad-spectrum antibacterial potential. Against fungal pathogens, the extract showed zones of 16±0.14 mm for Aspergillus niger and 18±0.24 mm for Penicillium species. CuO NPs exhibited weaker but consistent antibacterial effects, with inhibition zones ranging from 20±0.19 mm (S. aureus) to 24±0.26 mm (E. coli), while antifungal activity was modest (19±0.22 mm for A. niger and 23±0.16 mm for Penicillium spp.). In contrast, the nanoscaffolds displayed superior antimicrobial performance, achieving 29±0.17 mm (E. coli), 27±0.26 mm (K. pneumoniae), 24±0.14 mm (S. aureus), and 25±0.32 mm (C. koseri), along with 24±0.41 mm (A. niger) and 26±0.22 mm (Penicillium spp.). While ciprofloxacin (antibacterial) and voriconazole (antifungal) controls showed

higher efficacy (26±0.65 mm to 33±0.58 mm), the nanoscaffolds emerged as a promising composite with enhanced and sustained antimicrobial activity, likely due to the synergistic effects of CuO NPs and the polymeric matrix.

Table 1: Antimicrobial activity of Dictyota extract, CuO NPs, and starch/PVA electrospun nanoscaffolds at concentration of 50 µg/mL against various pathogenic organisms.

S. No	Organism	Zone of inhibition (mm)				
		Ciprofloxacin (Antibiotic)	Voriconazole (Antifungal)	Algal Extract	CuO NPs	Nano-scaffolds
1.	*Escherichia coli*	33±0.58	-	18±0.18	24±0.26	29±0.17
2.	*Klebsiella pneumoniae*	30±0.14	-	16±0.32	23±0.15	27±0.26
3.	*Staphylococcus aureus*	28±0.32	-	14±0.13	20±0.19	24±0.14
4.	*Citrobacter koseri*	29±0.47	-	18±0.12	22±0.13	25±0.32
5.	Aspergillus niger	-	26±0.65	16±0.14	19±0.22	24±0.41
6.	Penicillium species	-	28±0.39	18±0.24	23±0.16	26±0.22

4. DISCUSSION

The comprehensive characterization of CuO NPs synthesized using Dictyota extract and their subsequent integration into starch/PVA nanoscaffolds demonstrates their potential for biomedical applications, particularly as antimicrobial agents in wound healing and infection control. Each analytical technique employed provided critical insight into the physicochemical and functional attributes of the nanocomposite material [19].

UV–Visible spectroscopy played a pivotal role in establishing the successful synthesis of CuO NPs. The Dictyota extract exhibited a broad absorption band without distinct peaks, suggestive of the presence of biomolecules like polyphenols and flavonoids. These compounds are known to act as reducing and capping agents during nanoparticle biosynthesis. The CuO NPs, in contrast, showed a distinct surface plasmon resonance (SPR) peak around 270–300 nm, a hallmark of CuO nanostructures. This sharp peak, absent in the plant extract, confirmed the formation of CuO NPs and implied their stability in the colloidal state due to biomolecular capping. The increase in absorbance at higher wavelengths further validated the formation of metallic oxide nanoparticles, distinguishing them from the bioextract and confirming the transformation induced by the green synthesis method [34-37].

FTIR spectroscopy provided a detailed understanding of the functional groups involved in the synthesis and stabilization of CuO NPs, as well as their incorporation into the polymeric matrix. The FTIR spectrum of CuO NPs revealed peaks characteristic of Cu–O stretching vibrations, confirming the formation of copper oxide. Additionally, the presence of peaks corresponding to hydroxyl and carboxyl groups from the extract indicated successful capping. The starch/PVA scaffold, both with and without CuO NPs, showed strong O–H and C–O–C stretching vibrations, signifying the polymer's structural integrity. Importantly, the absorption bands between

600–400 cm^{-1} in the nanocomposite spectrum confirmed successful embedding of CuO NPs, suggesting interactions between the polymer and metal oxide through hydrogen bonding or electrostatic attraction, which are crucial for the stability and functionality of the composite [38, 39].

XRD analysis corroborated the crystallographic identity of the CuO NPs and their successful incorporation into the nanoscaffold. The distinct peaks observed for the CuO NPs matched well with the standard monoclinic phase (JCPDS No. 48-1548), affirming their crystalline nature. The presence of specific peaks in the scaffold spectrum related to CuO confirmed their integration without altering the base polymer's structure. The observed peak broadening in the nanoscaffold suggested a slight reduction in crystallinity, likely due to polymer-nanoparticle interactions that disrupt orderly polymer alignment. Nonetheless, the retention of key crystalline peaks implied that the structural integrity of the nanoparticles was preserved post-integration, which is essential for maintaining their functional efficacy [40, 41].

SEM images revealed detailed morphological features of both the synthesized CuO NPs and the nanoscaffolds. The CuO NPs were predominantly spherical with occasional agglomeration, a common phenomenon due to high surface energy. In contrast, the CuO-loaded starch/PVA scaffolds exhibited a well-defined fibrous morphology with uniform distribution of nanoparticles. The visible bright spots on the fiber surface corresponded to CuO NPs, indicating even dispersion within the matrix. The smooth fiber texture and consistent diameter distribution confirmed that electrospinning parameters were optimized. These observations are critical, as uniform distribution of nanoparticles within the scaffold ensures consistent functional performance, such as mechanical reinforcement and antimicrobial activity [42].

TGA provided insights into the thermal stability of the nanocomposite. The CuO-loaded scaffold showed a multi-step degradation pattern, with initial weight loss due to moisture evaporation, followed by major degradation attributed to polymer decomposition. Notably, the presence of CuO NPs delayed the onset of thermal degradation, indicating their role as thermal stabilizers. The final residue at high temperatures further confirmed the presence of inorganic content, i.e., CuO, providing evidence of their reinforcing capability. This enhanced thermal stability

is desirable for biomedical applications, particularly in scenarios involving sterilization or exposure to elevated temperatures [43-45].

Zeta potential and particle size analysis through DLS furnished vital data regarding the colloidal behavior and stability of the biosynthesized CuO NPs. The average particle size of approximately 92.8 nm with a moderate polydispersity index (PDI = 0.688) suggested a heterogeneous size distribution, likely due to partial aggregation. The zeta potential value of −20.08 mV, with peaks at −37.52 mV and −16.29 mV, indicated moderate colloidal stability. The dominant negative surface charge facilitated electrostatic repulsion among particles, helping to prevent severe aggregation, although the presence of a lower zeta potential population suggested some instability. Nonetheless, the negative charge is favorable for biocompatibility, as it reduces nonspecific interactions with cells and proteins [46-49].

Finally, the antimicrobial assessment illustrated the superior efficacy of the CuO-loaded starch/PVA scaffolds compared to individual components. While the Dictyota extract showed moderate activity and CuO NPs exhibited enhanced effects, their combination within the scaffold led to significantly improved inhibition zones across all tested bacterial and fungal strains. The nanoscaffold's efficacy, approaching that of standard antibiotics like ciprofloxacin and antifungals like voriconazole, can be attributed to the synergistic action between the polymer matrix and CuO NPs. The sustained release and high surface area of the nanoscaffold likely facilitate prolonged interaction with microbial cells, enhancing antimicrobial performance. These findings position the nanocomposite as a promising material for biomedical applications, particularly in antimicrobial wound dressings and infection-resistant implants [50, 51]. The results confirm that CuO NPs synthesized via a green route using Dictyota extract can be successfully integrated into starch/PVA nanofibrous scaffolds. The resultant composite demonstrates favorable physicochemical properties, structural stability, thermal resistance, and significant antimicrobial activity, highlighting its potential in biomedical and therapeutic domains.

5. CONCLUSION

This study successfully demonstrated the green synthesis of CuO NPs using Dictyota spp. extract and their effective incorporation into starch/PVA-based electrospun nanoscaffolds. UV–Vis spectroscopy confirmed nanoparticle formation via surface plasmon resonance, while FTIR and XRD analyses validated the presence of Cu–O bonds and crystalline structure, respectively. SEM imaging revealed uniform nanoparticle distribution within the nanofibrous matrix, and TGA showed enhanced thermal stability due to CuO reinforcement. DLS and zeta potential analysis indicated moderate stability with nanoscale particle size. Importantly, the CuO-integrated scaffolds exhibited superior antimicrobial activity against a range of bacterial and fungal pathogens compared to the individual extract and nanoparticles. These results collectively highlight the potential of Dictyota-mediated CuO nanocomposites as bioactive, thermally stable, and structurally robust materials for biomedical applications, particularly in wound healing and antimicrobial therapies. Future research should explore in vivo efficacy and long-term biocompatibility for clinical translation.

Data Availability Statement: The full dataset of physiochemical characterization associated with this work is published in Mendeley Data [Dataset] Multidisciplinary evaluation of biofabricated starch nanoscaffolds incorporating phyto-synthesized CuO nanoparticles from Dictyota extract (DOI: 10.17632/xtwhbc25hj.1).

Disclosure: The material characterization data and figures (e.g., UV, SEM, FTIR, XRD, TGA, Zeta Potential and particle sizer) presented here were generated from a common dataset and are being reused across multiple related studies on nanomaterials. All biological analyses and conclusions are original to each manuscript.

Conflicts of Interest: The authors declare no conflicts of interest.

REFERENCES

1. Ganesan A, Kumar NG, Natarajan PM. Anticancer activity of silver nanoparticles synthesized from aqueous Chellamanimegalai P, Deshmukhe G, Balange AK, Layana P. Unveiling the nutritional and antioxidant properties of brown algae resources (Dictyota JV Lamouroux) from the Bay of Bengal and Arabian Sea, Indian coast. Heliyon. 2025; 11 (1): e40693.
2. Surendran N, Chandrasekaran G, Raju MV, Chandrasekaran MK, Ahalliya RM, Palanisamy CP, Kanniappan GV, Arcot R, Alharbi NS, Thiruvengadam M. Anti-inflammatory potential of ethanolic extract of Maranta arundinacea L.: Insights from COX-2 modulation and oxidative stress analysis. South African Journal of Botany. 2026; 195: 142-151.
3. Pei J, Senthilkumar MV, Hessini K, Subramaniyam S, Sivaramakrishnan R, Kanniappan GV, Jayaraman S, Palanisamy CP. Green fabrication of starch/PVA/CuO nanoscaffolds using marine macroalgae extract for enhanced anti-inflammatory activity. Sustainable Chemistry and Pharmacy. 2026; 51: 102397.
4. Balasubramanian V, Loganathan L, Muthuswamy K, Viswanathan TM, Raju MV, Chandrasekaran MK, Ahalliya RM, Poorasamy J, Palanisamy CP, Dominic S, Kanniappan GV. Anticancer therapeutic efficacy of PEGylated β-galactosidase from Aspergillus terreus in DMBA-induced breast cancer: Toxicological, molecular and histopathological evaluation in Wistar rats. International Journal of Biological Macromolecules. 2026; 360: 151856.

5. Jayaraman S, Eswaran A, Rajagopal P, Palanisamy CP, Veerakumar P, Veeraraghavan VP, Sirasanagandla SR. Neuroendocrine-associated epigenetic factors in cellular senescence: mechanisms and therapeutic implications. Biogerontology. 2026; 27(2): 64.
6. Ponnusamy B, Rajagopal P, Palanisamy CP, Veeraraghavan VP, Jayaraman S. Mechanistic Exploration of the anticancer activity of Justicia adhatoda Plant Leaf Ethanolic Extract against Colon Cancer Cells: An in silico and in vitro Approach. Asian Pacific Journal of Cancer Prevention. 2026; 27(3): 1069-1080.
7. Pei J, Saran VS, Sivaramakrishnan R, Kanniappan GV, Pandurangan V, Jayaraman S, Dhayalan VK, Mironescu M, Mironescu ID, Palanisamy CP. Ultrasonic-assisted, Sargassum ilicifolium (brown marine macroalgae)-mediated biogenic synthesis of CuO nanoparticles incorporated in starch/PVA electrospun nanoscaffolds: In vitro safety and antioxidant efficacy assessment. Bioorganic Chemistry. 2026; 173: 109679.
8. Raj MAPA, Subramaniyam S, Kanniappan GV, Jayaraman S, Palanisamy CP. Sustainable fabrication of starch/PVA/CuO electrospun nanoscaffolds from Turbinaria ornata (marine macroalgae) extract: Physicochemical characterization and antidiabetic evaluation. Kuwait Journal of Science. 2026; 53(2): 100545.
9. Pei J, Ganesh NS, Subramaniyam S, Sivaramakrishnan R, Kanniappan GV, Jayaraman S, Palanisamy CP. Sustainable fabrication of starch/PVA/CuO electrospun nanoscaffolds from Padina tetrastromatica (Brown macroalgae) extract: Physicochemical characterization and antidiabetic assessment. Sustainable Chemistry One World. 2026; 9: 100195.
10. Sakthiraj A, Sivaramakrishnan R, Subramaniyam S, Kanniappan GV, Pandurangan V, Jayaraman S, Dhayalan VK, Mironescu M, Mironescu ID, Palanisamy CP. Chemical Physics Impact. Starch/PVA electrospun nanoscaffolds loaded with ultrasonic-assisted green-synthesis of CuO nanoparticles from marine macroalgae (Gracilaria corticata) extract: Cytotoxicity and antioxidant analysis. 2026; 12: 101018.
11. Raju M, Chandrasekaran MK, Loganathan L, Ahalliya RM, Mironescu M, Mironescu ID, Palanisamy CP, Kanniappan GV. Lipid remodeling and ferroptosis in phosphatidylcholine-mediated tumor–stroma crosstalk. Frontiers in Molecular Biosciences. 2026; 13: 1742305.
12. Kunamalla R, Panagal M, Palanisamy CP. Biogenic synthesis and fabrication of starch/PVA/CuO electrospun nanoscaffolds from Sargassum ilicifolium (brown marine macroalgae) extract for anticancer activity on HT-29 and MCF-7 cancer cells. Biocatalysis and Agricultural Biotechnology. 2026; 72: 103923.
13. Pei J, Govindaraj H, Sivaramakrishnan R, Kanniappan GV, Pandurangan V, Dhayalan VK, Mironescu M, Mironescu ID, Jayaraman S, Palanisamy PC. Sustainable fabrication of biopolymer-based (starch/PVA) nanoscaffolds loaded with green-synthesized CuO nanoparticles from Sargassum wightii (marine macroalgae): Cytocompatibility and antioxidant activity. Biomaterials Advances. 2026; 182: 214660.
14. Pei J, Perumal NC, Meng P, Long Q, Palanisamy CP. Extracellular vesicle-based biosensors for Alzheimer's disease: A new frontier in precision diagnostics. Ageing Research Reviews. 2026; 113: 102904.
15. Shree P, Sivaramakrishnan R, Kanniappan GV, Pandurangan V, Jayaraman S, Dhayalan VK, Mironescu M, Mironescu ID, Palanisamy CP. Antioxidant and biocompatible CuO-starch/PVA nanoscaffolds via ultrasonic green synthesis using Turbinaria conoides (brown marine macroalgae). Medicine in Drug Discovery. 2025; 28: 100238.
16. Gong J, Lin J, Guan T, Pei J, Palanisamy CP, El-AtyFrom AMA. selenium tolerance to nanoplastic antagonism: Comprehensive characterization of L. casei SNUT1 and its extracellular vesicle–nanoselenium complex. Food Bioscience. 2025; 74: 107749.
17. Poochi SP, Sundarraj R, Raju MV, Chandrasekaran MK, Ahalliya RM, Palanisamy CP, Kanniappan GV, Kondapavuluri BK, Thiruvengadam M. Harnessing Nature: Computational and Experimental Insights Into Ipomoea obscura Metabolites for Bladder Cancer Therapy. Chemistry and Biodiversity. 2025; 0: e00909.
18. Dugganaboyana GK, Kannankumar MKG, Shivaramakrishna S, Raju MV, Chandrasekaran MK, Ahalliya RM, Panneerselvam N, Palanisamy CP, Kanniappan GV. Phytochemical insights, antioxidant activity and therapeutic potential of Cassia senna against prostate cancer in Wistar albino rats. Discover Applied Sciences. 2025; 7:1206.
19. Natarajan SR, Krishnamoorthy R, Alshuniaber MA, Gatasheh MK, Rajagopal P, Veeraraghavan VP, Palanisamy CP, Jayaraman S. KDM1A Facilitates Oncogenic Potential in Colorectal Cancer Progression Through the Activation of AXIN/GSK3β/β-Catenin Signaling Pathways: Evidence From Integrated Transcriptomics and In Vitro Studies. The Journal of Gene Medicine. 2025; 27(11): e70053.
20. Guan T, Gong J, Lin J, Palanisamy CP, Jinjin Pei J, El-Aty AMA. Machine learning-driven multimodal optimization of selenium biotransformation and flavor profiling in fermented apple–Yacon functional beverages. Innovative Food Science & Emerging Technologies. 2025; 105: 104198.
21. Natarajan SR, Krishnamoorthy R, Alshuniaber MA, Alsulami TS, Gatasheh MK, Rajagopal P, Palanisamy CP, Govindan R, Veeraraghavan VP, Jayaraman S. ABCE1 facilitates tumour progression via aerobic glycolysis and inhibits cell death in human colorectal cancer cells through the p53 signalling pathway. Scientific Reports. 2025; 15: 24674.
22. Huang Y, Guo H, Liu Y, Jin W, Palanisamy CP, Pei J, Oz F, El-Aty AMA. Effects of Natural Polysaccharides on the Gut Microbiota Related to Human Metabolic Health. Molecular Nutrition & Food Research. 2025; 69:e202400792.
23. Poornima K, Meenakshi K.C, Manikandan V.R, Shankari G, Prabhu D, Rathi M.A, Palanisamy CP, Balaji R, Gopalakrishnan V.K. Exploring the anticancer potential of Jerantinine A from Tabernaemontana coronaria against

prostate, breast, and ovarian cancers: A computational approach. Journal of Complementary and Integrative Medicine, 2025 22(2): 363–372.
24. Palanisamy CP, Poompradub S, Sansanaphongpricha K, Jayaraman S, Subramani K. Faridah Sonsudin gGreen synthesis of Nigella sativa-mediated silver nanoparticles for enhanced antibacterial activity and wound healing: Mechanistic insights and biomedical applications. Environmental Nanotechnology, Monitoring & Management. 2025; 24: 101085.
25. Surendran N, Raju MV, Chandrasekaran MK, Ahalliya RM, Palanisamy CP, Chandrasekaran G, Kanniappan GV. Physicochemical characterization of starch from Maranta arundinacea L.(arrowroot) rhizomes and its inhibition of COX-2: In vivo validation. Bioactive Carbohydrates and Dietary Fibre. 2025; 33: 100465.
26. Kannappan P, Chandrasekaran MK, Raju MV, Gopalakrishnan S, Dhamodharan P, Ahalliya RM, Palanisamy CP, Raju B, Kanniappan GV. Exploring the anticancer potential of Jerantinine A from Tabernaemontana coronaria against prostate, breast, and ovarian cancers: a computational approach. Journal of Complementary and Integrative Medicine. 2025; 22(02): 363-372.
27. Pei J, Kumarasamy RV, Jayaraman S, Kanniappan GV, Long Q, Palanisamy CP. Quercetin-functionalized nanomaterials: Innovative therapeutic avenues for Alzheimer's disease management. Ageing Research Reviews. 2025; 104: 102665.
28. Jayaraman S, Prasad M, Natarajan SR, Krishnamoorthy R, Alshuniaber MA, Gatasheh MK, Veeraraghavan VP, Rajagopal P, Palanisamy CP. Molecular mechanisms underlying the effects of beta-sitosterol on TGF-β1/Nrf2/SIRT1/p53-mediated signaling in the kidney of a high-fat diet and sucrose-induced type-2 diabetic rat. Chemico-Biological Interactions. 2025; 411: 111443.
29. Huang Y, Guo H, Liu Y, Jin W, Palanisamy CP, Pei J, Oz F, El-Aty AMA. Effects of Natural Polysaccharides on the Gut Microbiota Related to Human Metabolic Health. Molecular Nutrition & Food Research. 2025; e202400792.
30. Prabhakaran P, Palanisamy CP, Shanmugam A, Damodharan P, Swaminathan H, Devaraj D, Ahalliya RM, Kanniappan GV. Isolation, structural characterization, and molecular docking studies on the bioactive compound from n-Hexane extract of Emilia sonchifolia (L.) DC against the pancreatic cancer target Aurora 2 Kinase. Journal of Complementary and Integrative Medicine. 2024; 22(1): 0290.
31. Jiang H, Kumarasamy RV, Pei J, Raju K, Kanniappan GV, Palanisamy CP. Integrating engineered nanomaterials with extracellular vesicles: Advancing targeted drug delivery and biomedical applications. Frontiers in Nanotechnology. 2024; 6: 1513683.
32. Guo H, Liu Y, Wan T, Song D, Palanisamy CP, Geng J, Pei J, Özmen S, El-Aty AMA. Toward personalized cancer management: Role of precision nutrition–diet interventions. Journal of Functional Foods. 2024; 123: 106584.
33. Natarajan SR, Krishnamoorthy R, Alshuniaber MA, Al-Anazi KM, Farah MA, Rajagopal P, Palanisamy CP, Veeraraghavan VP, Jayaraman S. Identification of FOXM1 as a novel protein biomarker and therapeutic target for colorectal cancer progression: Evidence from immune infiltration and bioinformatic analyses. International Journal of Biological Macromolecules. 282 (Part 4): 137201.
34. Rajendran MS, Jayaraman S, Khan JM, Jasmine S, Prabhakaran RK, Raju MV, Chandrasekaran MK, Ahalliya RM, Kannappan P, Palanisamy CP, Kanniappan GV. Investigating the colon toxicity and carcinogenic role of monosodium glutamate compared with Dimethylhydrazine in male Wistar rats: Exploring the link to childhood colon cancer risk. Journal of King Saud University - Science. 2024; 36(11): 103507.
35. Kumarasamy RV, Natarajan PM, Umapathy VR, Roy JR, Rab SO, Saeed M, Panagal M, Mironescu M, Srinivasan GP, Palanisamy CP. Clinical Applications and Therapeutic Potentials of Advanced Nanoparticles: A Comprehensive Review on Completed Human Clinical Trials. Frontiers in Nanotechnology. 2024; 6:1479993.
36. Jin W, Pei JJ, Roy JR, Jayaraman S, Ahalliya RM, Kanniappan GV, Mironescu M, Palanisamy CP. Comprehensive review on single-cell RNA sequencing: A new frontier in Alzheimer's disease research. Ageing Research Reviews. 2024; 274: 102454.
37. Pei J, Palanisamy CP, Jayaraman S, Natarajan PM, Umapathy VR, Roy JR, Panagal M, Jayaraman S. Curcumin-loaded polymeric nanomaterials as a novel therapeutic strategy for Alzheimer's disease: A comprehensive review. Ageing Research Reviews. 2024; 99: 102393.
38. Pei J, Palanisamy CP, Jayaraman S, Natarajan PM, Umapathy VR, Roy JR, Thalamati D, Ahalliya RM, Kanniappan GV*, Mironescu M. A comprehensive review on starch-based Sustainable Edible Films Loaded with Bioactive Components for Food Packaging. International Journal of Biological macromolecules. 2024; 274 (Part-1): 133332.
39. Palanisamy CP, poompradub S, Sansanaphongpricha K, Subramani K, Sonsudin F. Increased expression levels of PDGF and VEGF magnify the wound healing potential facilitated by biogenic synthesis of silver nanoparticles. Nano-Structures & Nano-Objects. 2024; 39: 101236.
40. Pei J, Palanisamy CP, Jayaraman S, Natarajan PM, Umapathy VR, Roy JR, Thalamati D, Ahalliya RM, Kanniappan GV, Mironescu M. Proteomics Profiling of Extracellular Vesicle for Identification of Potential Biomarkers in Alzheimer's Disease: A Comprehensive Review. Ageing Research Reviews. 2024; 99: 102359.
41. Xi J, Wang T, Xian P, Liu X, Du M, Yang H, Palanisamy CP, Lin W, Long Q. Proteomic insights uncover enhanced neurotherapeutic potential in conditioned mesenchymal stem cell-derived extracellular vesicles. Extracellular Vesicle. 2024; 3: 100037.

42. Pei J, Natarajan PM, Umapathy VR, Swamikannu B, Sivaraman NM, Krishnasamy L, Palanisamy CP. Advancements in the synthesis and functionalization of zinc oxide-based nanomaterials for enhanced oral cancer therapy. Molecules. 2024; 29(11): 2706.
43. Gatasheh MK, Natarajan SR, Krishnamoorthy R, Alsulami TS, Rajagopal P, Palanisamy CP, Veeraraghavan VP, Jayaraman S. Molecular analysis to identify novel potential biomarkers as drug targets in colorectal cancer therapy: an integrated bioinformatics analysis. Molecular and Cellular Oncology. 2024; 11(1): 2326699.
44. Pei J, Yan Y, Jayaraman S, Rajagopal P, Natarajan PM, Umapathy VR, Gopathy S, Roy JR, Sadagopan CS, Thalamati D, Palanisamy CP, Mironescu M. A review on advancements in the application of starch-based nanomaterials in biomedicine: Precision drug delivery and cancer therapy. International Journal of Biological Macromolecules. 2024; 130746.
45. Pei JJ, Yan Y, Palanisamy CP, Jayaraman S, Natarajan PM, Umapathy VR, Gopathy S, Roy JR, Sadagopan JC, Thalamati D, Mironescu M. Materials-based drug delivery approaches: Recent advances and future perspectives. Green Processing and Synthesis. 2024; 13: 20230094.
46. Panneerselvam S, Viswaja K, Deepa E, Prathiba S, Rebecca FS, Nivedha RP, Rajagopal P, Veeraraghavan VP, Sridevi G, Palanisamy CP, Jayaraman S. Hypoglycemic Potential of Acalypha indica in Streptozotocin-Induced Type 2 Diabetic Rats. International Journal of Drug Delivery Technology. 2026; 16(26s):1038-1047.
47. Panneerselvam S, Viswaja K, Prathiba S, Rebecca FS, Nivedha RP, Rajagopal P, Fathima SJH, Veeraraghavan VP, Sridevi G, Palanisamy CP, Jayaraman S. Acalypha Indica Attenuates Insulin Resistance in STZ-Induced Type 2 Diabetic Male Rats: Mechanistic Study. International Journal of Drug Delivery Technology. 2026; 16(26s):1027-1037.
48. Manju NE, Natarajan A, Rebecca FS, Nivedha RP, Hemalatha R, Rajagopal P, Murali R, Veeraraghavan VP, Sridevi G, Palanisamy CP, Jayaraman S. Effect of Seendhil polyherbal formulation in attenuating type-2 diabetes in STZ-induced experimental rats. International Journal of Drug Delivery Technology. 2026; 16(26s):981-989.
49. Manju NE, Natarajan A, Rebecca FS, Nivedha RP, Hemalatha R, Rajagopal P, Murali R, Veeraraghavan VP, Sridevi G, Palanisamy CP, Jayaraman S. Molecular mechanism to identify the effects of Seendhil polyherbal preparation on IRS-1/AKT/GLUT4/NRF2-KEAP-1 mediated signaling in SFZ-induced type-2 diabetic adult male rats. International Journal of Drug Delivery Technology. 2026;16(26s):972-980.
50. Palanisamy CP, Poompradub S, Sansanaphongpricha K, Jayaraman S, Subramani K, Sonsudin F. Biosynthesis of silver nanoparticles (AgNPs) using ethanolic extract of Nigella sativa (L.) seeds promotes wound healing via PDGF and VEGF signalling pathways activation. Biocatalysis and Agricultural Biotechnology. 2023; 54: 102970.
51. Palanisamy CP, Pei JJ, Phaniendra A, Venkata AAN, Jayaraman S, Veeraragahavan VP, Sridevi G, Roy JR, Janaki CS, Thalamati D, Mironescu M, Luo Q, Chai Y, Long Q. New Strategy of Neurodegenerative Disease Treatment with Extracellular Vesicles (EVs) Derived from Mesenchymal Stem Cells (MSCs). Theranostics. 2023; 13(12):4138-4165.